Symmetric and asymmetric solitons and vortices in linearly coupled two-dimensional waveguides with the cubic-quintic nonlinearity

Nir Dror and Boris A. Malomed

Department of Physical Electronics, School of Electrical Engineering,
Faculty of Engineering, Tel Aviv University, Tel Aviv 69978, Israel

It is well known that the two-dimensional (2D) nonlinear Schrödinger equation (NLSE) with the cubic-quintic (CQ) nonlinearity supports a family of stable fundamental solitons, as well as solitary vortices (alias vortex rings), which are stable for sufficiently large values of the norm. We study stationary localized modes in a symmetric linearly coupled system of two such equations, focusing on *asymmetric* states. The model may describe "optical bullets" in dual-core nonlinear optical waveguides (including *spatiotemporal vortices* that were not discussed before), or a Bose-Einstein condensate (BEC) loaded into a "dual-pancake" trap. Each family of solutions in the single-component model has two different counterparts in the coupled system, one symmetric and one asymmetric. Similarly to the earlier studied coupled 1D system with the CQ nonlinearity, the present model features *bifurcation loops*, for fundamental and vortex solitons alike: with the increase of the total energy (norm), the symmetric solitons become unstable at a point of the direct bifurcation, which is followed, at larger values of the energy, by the *reverse bifurcation* restabilizing the symmetric solitons. However, on the contrary to the 1D system, both the direct and reverse bifurcation may be of the subcritical type, at sufficiently small values of the coupling constant, λ. Thus, the system demonstrates a *double bistability* for the fundamental solitons. The stability of the solitons is investigated via the computation of instability growth rates for small perturbations. Vortex rings, which we study for two values of the "spin", $s = 1$ and 2, may be subject to the azimuthal instability, like in the single-component model. In particular, complete destabilization of asymmetric vortices is demonstrated for a sufficiently strong linear coupling. With the decrease of λ, a region of stable asymmetric vortices appears, and a single region of bistability for the vortices is found. We also develop a quasi-analytical approach to the description of the bifurcations diagrams, based on the variational approximation. Splitting of asymmetric vortices, induced by the azimuthal instability, is studied by means of direct simulations. Interactions between initially quiescent solitons of different types are studied too. In particular, we confirm the prediction of the reversal of the sign of the interaction (attractive/repulsive for in-phase/out-of-phase pairs) for the solitons with the odd spin, $s = 1$, in comparison with the even values, $s = 0$ and 2.

I. INTRODUCTION

In the last two decades, much interest has been drawn to the studies of spatiotemporal solitons (STSs, alias "light bullets") in nonlinear optics [1, 2]. They are supported through the balance between the temporal dispersion, spatial diffraction, and nonlinearity. It is well known that two-dimensional (2D) and three-dimensional (3D) STSs cannot be stable in uniform media with the cubic (Kerr) nonlinearity, due to possibility of the collapse in the same setting [2, 3]. To avoid the collapse, other types of the nonlinearity were proposed. In particular, the stability of multidimensional solitons is readily secured by saturable [4, 5], quadratic ($\chi^{(2)}$) [6, 7], and cubic-quintic (CQ) nonlinearities [8, 9]. While the creation of STSs in 3D has not been reported so far, quasi-2D STSs were made in $\chi^{(2)}$ crystals [10].

While the fundamental (zero-vorticity) STSs supported by the above-mentioned non-Kerr nonlinearities are stable, the stability of solitary vortices (alias vortex rings, or spinning solitons, with integer "spin" s referring to the corresponding topological charge) are vulnerable to the destabilization by azimuthal perturbations. In particular, spinning solitons in 2D models with $\chi^{(2)}$ or saturable nonlinearity are unstable, as demonstrated by simulations [11] and the experiment [12]. The azimuthal instability breaks the solitary vortices with $s = 1$ into two or three fragments, each re-trapping into a moving fundamental soliton, so that the intrinsic spin moment of the unstable mode is transformed into the orbital momentum of the set of separating fragments.

Vortex solitons may be stable in media with *competing nonlinearities*. In particular, stable 2D vortices, with $s = 1$ and 2, were found in a model combining the $\chi^{(2)}$ and self-defocusing cubic nonlinearities [13]. Another model which is known to support stable 2D spinning solitons includes self-focusing cubic and self-defocusing quintic nonlinearities. Quiroga-Teixeiro and Michinel [14] were the first to demonstrate in direct simulations that 2D solitons with $s = 1$ may be stable in the CQ model, provided that their power (norm) is sufficiently large. The detailed analysis [15, 16], which made use of the linearized version of the model for computing growth rates of perturbation eigenmodes, had demonstrated that, for spins $s = 1$ and 2, the CQ model exhibits relatively large stability regions, which cover, respectively, $\approx 9\%$ and $\approx 8\%$ of the respective existence regions, in terms of soliton's norm (total power). It has also been demonstrated that the spinning solitons with the vorticity up to $s = 5$ may also be stable, but in extremely narrow regions [17].

The subject of the present work are 2D solitons, both the fundamental and spinning ones, in a symmetric system of two linearly coupled nonlinear Schrödinger equations (NLSEs) with the CQ nonlinear terms. The main objectives of the analysis are the *symmetry-breaking bifurcations* and asymmetric solitons generated by them. As explained below, the model may have realizations in both nonlinear optics and BECs (Bose-Einstein condensates, where the NLSE is known as the Gross-Pitaevskii equation, GPE [18]). The 1D version of the model was studied in Ref. [19], where it was found that a bifurcation of the supercritical type destabilizes symmetric two-component solitons, generating a pair of asymmetric ones. At larger values of the norm (power), the branches of symmetric and asymmetric solitons merge back, restabilizing the symmetric ones, which gives rise to a *bifurcation loop*. At relatively small values of the linear-coupling constant, λ, the reverse bifurcation is of the subcritical type, which may feature a large region of the bistability between the symmetric and asymmetric 1D solitons. With the increase of λ, the bistability region gradually disappears and the bifurcation loop shrinks, vanishing and leaving only the symmetric solitons in the system at still larger values of λ.

Spontaneous-symmetry-breaking bifurcations of 2D solitons and vortices in linearly-coupled systems were studied in Ref. [20], in terms of two parallel pancake-shaped BECs linked by the tunneling of atoms across the potential barrier separating them. The model was based on two GPEs with the linear coupling and cubic nonlinearity. The stability of the solitons and vortices against the collapse and (as concerns the vortices) against the splitting was provided by a 2D periodic potential (an optical lattice) present in both equations. In agreement with the results known from other models, the symmetric solitons and vortices underwent the symmetry-breaking bifurcations in the system with the self-attractive nonlinearity. Unlike that setting, in the present work we consider the uniform space, the stability of the single-component solitons and vortices being provided by the CQ nonlinearity.

The paper is organized as follows. The model is introduced, and its physical realizations are discussed, in section II. The set of stationary solutions to the coupled equations is parameterized by the linear-coupling constant, λ, and the propagation coefficient, k. In section III we present asymmetric solutions, and produce bifurcation diagrams for the fundamental and spinning solitons, with vorticities $s = 0, 1, 2$. Section IV reports a detailed stability analysis, performed by dint of numerical calculations of the growth rates for eigenmodes of small azimuthal perturbations. In section V, we develop an explicit analytical approximation for the solutions, based on the variational method. Results of direct numerical simulations, which demonstrate the splitting of azimuthally unstable asymmetric spinning solitons, are displayed in section VI. In section VII we report numerical results for interactions between solitons. The paper is concluded by section VIII.

II. THE MODEL

The system of 2D linearly coupled equations with the CQ nonlinearity is taken in the scaled form (cf. the 1D system introduced in Ref. [19]):

$$
i\psi_z + \psi_{xx} + \psi_{yy} + |\psi|^2\psi - |\psi|^4\psi = -\lambda\phi,
$$
$$
i\phi_z + \phi_{xx} + \phi_{yy} + |\phi|^2\phi - |\phi|^4\phi = -\lambda\psi. \tag{1}
$$

In the terms of the BEC, this is the system of GPEs for wave functions of the condensate in parallel tunnel-coupled pancake-shaped traps, with the negative scattering length accounting for the cubic self-attraction, the scattering length itself being eliminated by the rescaling [20]. In this context, evolution variable z is actually time, the quintic terms account for repulsive three-body collisions, provided that collision-induced losses may be neglected [21].

Actually, Eqs. (1) may find a more relevant interpretation in the application to optics, where the equations appear as normalized NLSEs for the transmission of spatiotemporal light signals in a dual-core planar waveguides. In this context, z is the propagation distance, x is the transverse coordinate, and y is the temporal variable (reduced time), provided that the sign of the group-velocity dispersion in the waveguide is anomalous [1]. Accordingly, terms ψ_{xx}, ϕ_{xx} and ψ_{yy}, ϕ_{yy} account for the paraxial diffraction and dispersion of light, respectively, while $1/\lambda$ determines the coupling length in the dual-core waveguide. The equations are made symmetric with respect to x and y by means of rescaling of the spatial and temporal variables. Also, λ is fixed to be real and positive, which can also be achieved in the general case by means of an obvious transformation. As for the self-focusing-defocusing CQ nonlinearity, it was theoretically predicted [22] and observed [23] in diverse optical media. Some of them admit the fabrication of dual-core planar waveguides.

The fundamental STS in a planar waveguide, although it has never been reported in an experiment, is a well-known concept [2]. On the other hand, the *spatiotemporal vortex*, whose snapshot would seem as an elliptic ring running at the speed of light in the plane of the waveguide, is a novel object. In the experiment, it may be coupled into the planar waveguide by an oblique vortical laser beam shone onto the waveguide under an appropriate angle. In that sense, the physical purport of the spatiotemporal vortices is essentially different from that of $(2+1)$-dimensional spatial solitons with the embedded vorticity, which are understood as hollow cylindrical beams of light propagating in a bulk medium [11–16]. In the experiment, vortical spatial solitons, built as multi-beam complexes with the phase distribution carrying the effective vorticity (rather than cylindrical beams), were created in photorefractive crystals with the saturable nonlinearity, their stability against splitting being maintained by a photoinduced lattice potential [24]).

We aim to find stationary axisymmetric solutions to Eqs. (1) as

$$
\psi = U(r)\exp(is\theta)\exp(ikz),
$$
$$
\phi = V(r)\exp(is\theta)\exp(ikz), \tag{2}
$$

where r and θ are the polar coordinates in the (x,y) plane, k is the propagation constant, and integer s is the above-mentioned spin. Substituting expressions (2) into Eqs. (1), we arrive at equations for real functions U and V:

$$
-kU + \frac{d^2U}{dr^2} + \frac{1}{r}\frac{dU}{dr} - \frac{s^2}{r^2}U + U^3 - U^5 = -\lambda V,
$$
$$
-kV + \frac{d^2V}{dr^2} + \frac{1}{r}\frac{dV}{dr} - \frac{s^2}{r^2}V + V^3 - V^5 = -\lambda U, \tag{3}
$$

with the boundary conditions demanding that the solution must feature asymptotic forms $r^{|s|}$ at $r \to 0$, and $\exp(-\sqrt{k}r)$ at $r \to \infty$ (hence k must be positive). The energies (norms) of the two components of the soliton (alias their norms) are defined as usual,

$$
E_{U,V} = 2\pi \int_{-\infty}^{+\infty} r(U^2, V^2)dr, \tag{4}
$$

the total energy being $E_{\text{total}} = E_U + E_V$. The asymmetry of the two-component soliton is characterized by ratio

$$
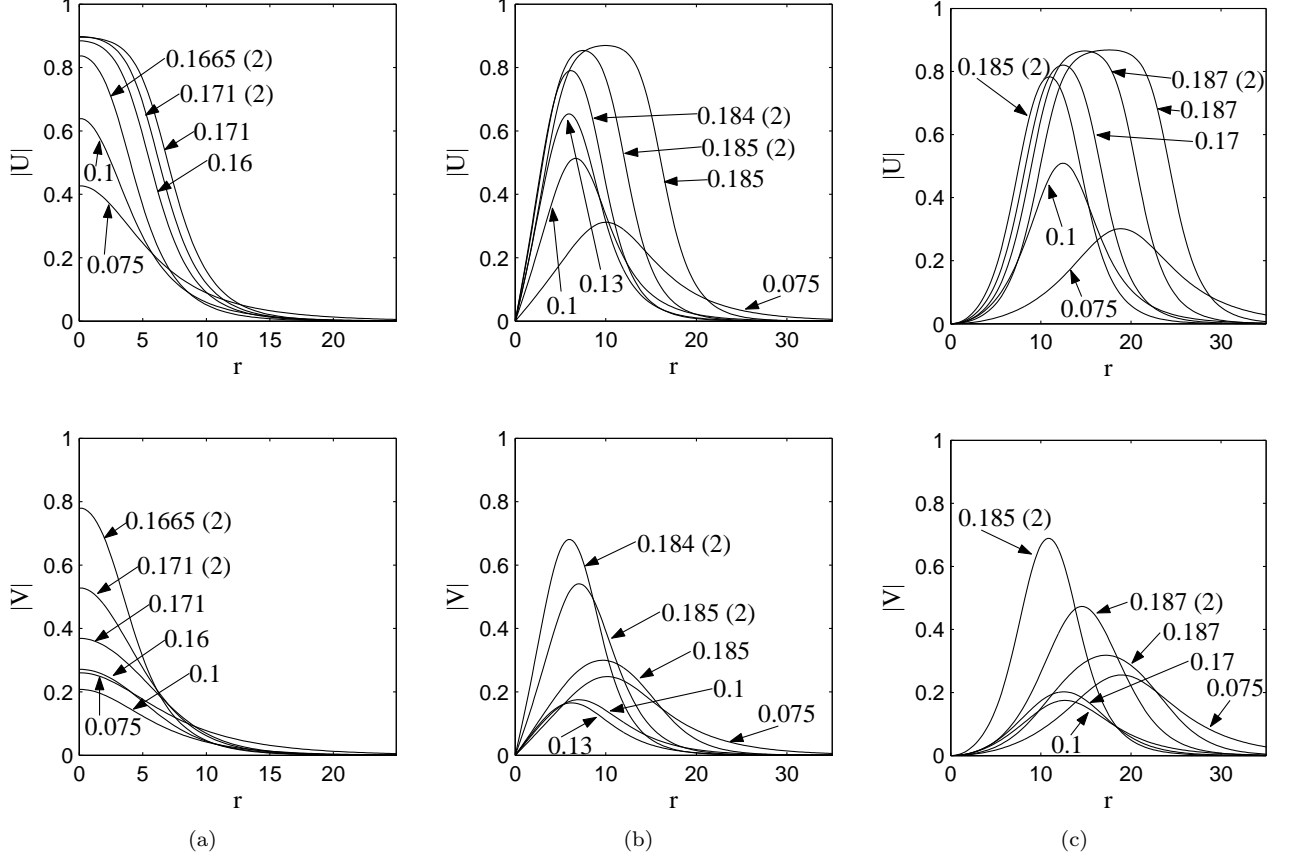\Theta = \frac{E_U - E_V}{E_U + E_V} \ . \tag{5}
$$

FIG. 1. Examples of asymmetric solitons with vorticities $s = 0$ (a), $s = 1$ (b), and $s = 2$ (c), for coupling constant $\lambda = 0.05$. Both components are shown, with values of propagation constant k indicated near the corresponding curves. Notice that in the (k, Θ) plane (Θ is the asymmetry measure defined as per Eq. (5)), families of the solutions form closed loops, which include the reverse bifurcation of the subcritical type, see Figs. 2-4 below. Therefore, asymmetric solutions are found for k increasing up to a certain maximum value, and then turning back and decreasing until hitting the reverse-bifurcation point. In the present panels, the solitons pertaining to the "backward" subfamily are labeled by (2), to distinguish them from their counterparts with the same values of k belonging to the "forward" part of the family.

III. ASYMMETRIC SOLITONS AND BIFURCATION LOOPS

Stationary symmetric and asymmetric soliton solutions for $s = 0, 1$ and 2 were generated in a numerical form, applying the Newton-Raphson method to Eqs. (3). We have also examined the possibility of the existence of elliptic solitons (i.e., anisotropic localized solutions to Eqs. (3)), using several numerical algorithms adjusted for the 2D setting, such as a generalized Petviashvili iteration method, and a modification of the squared-operator method presented in Ref. [25]. No stationary elliptic solutions have been found.

Symmetric soliton solutions in the present model, with $\psi = \phi$ and $\Theta = 0$, can be obtained from their counterparts previously found in the single-component CQ model, i.e., one equation from system (1), with $\lambda = 0$, for a single wave function, φ: $\psi(x, y, z; k) = \phi(x, y, z; k) \equiv \varphi(x, y, z; k - \lambda)$. Accordingly, the symmetric solutions emerge at $k = \lambda$, with the known minimum (threshold) values of the energy in the single component [16]: $E_{\text{thr}} = 11.73, 48.38$, and 88.34, for $s = 0, 1$, and 2, respectively. Within the family of the symmetric solitons, k varies from $k_{\min} \equiv \lambda$, which corresponds to $E = E_{\text{thr}}$, up to $k_{\max} = \lambda + 3/16$, corresponding to $E \to \infty$ ($k = 3/16$ is the value of the propagation constant in the single-component 2D model at which the energy diverges, along with the soliton's radius, for any s [15]).

For each value of the spin, a unique family of asymmetric solitons, with $U \neq V$ and $\Theta \neq 0$, can be found. Typical radial profiles of asymmetric solitons with $s = 0, 1$ and 2, for $\lambda = 0.05$ and several values of k, are shown in Fig. 1.

Similar to its 1D counterpart [19], the present system features bifurcation loops accounting for the transition from symmetric solitons to the asymmetric ones and back. Several generic examples of the bifurcation loops are shown in

Figs. 2, 3 and 4, for $s = 0, 1$ and 2, respectively. As in the 1D case, the loops shrink as the coupling constant, λ, increases, and they expand as λ decreases. In the limit of $\lambda \to 0$, the loops open up in the direction of $E \to \infty$.

For $s = 0$, the loop collapses and disappears at $\lambda_{\max}^{(s=0)} \approx 0.0964$. Up to $\lambda \approx 0.0852$, both the direct bifurcation and the reverse one, which closes the loop, are subcritical, giving rise to two regions of bistability (which may also be called *tristability*, as the asymmetric soliton always exists in two copies, which are specular images to each other). This bifurcation picture is different from the one obtained in the 1D model, in which the direct bifurcation is *always* supercritical. In the narrow interval of $0.0852 < \lambda < 0.0891$, the direct bifurcation in the present model is supercritical, while the reverse one remains subcritical. With the further increase of λ up to the point of the disappearance of the loop, $0.0891 < \lambda < 0.0964$, both the direct and reverse bifurcations are supercritical, and the loop's shape is completely convex, featuring no bistability.

The stability of all the branches of the fundamental ($s = 0$) solitons strictly follows criteria of the elementary bifurcation theory [27]. In particular, the branches generated by super- and subcritical bifurcations emerge as, respectively, stable and unstable ones, and the character of the stability changes when a branch passes a turning point. On the other hand, the *Vakhitov-Kolokolov criterion*, $dE/dk > 0$, which in many models with attractive nonlinearities is a necessary stability condition [1, 3, 4, 28], does not catch the instability of solitons related to the symmetry-breaking bifurcations, which is a known fact too [19, 20]. The stability properties are different for vortices, as they may be additionally unstable against azimuthal perturbations [15–17]. The analysis of the azimuthal instability of vortex solitons in the present model is reported in the next section.

As seen in Fig. 3, the bifurcation picture for $s = 1$ (without referring to the stability, for the time being) is very similar to that for $s = 0$. The solution branches form a loop, with both the direct and reverse bifurcations being subcritical in the interval of $0 < \lambda < 0.0998$. At $0.0998 < \lambda < 0.1018$, the direct bifurcation is supercritical, while the reverse one is still subcritical. The two bifurcations are supercritical, corresponding to the completely convex loop, at $0.1018 < \lambda < 0.110 \approx \lambda_{\max}^{(s=1)}$, up to the point where the bifurcation loop ceases to exist.

The bifurcation loops were also constructed for vortex solitons with spin $s = 2$. As seen in Fig. 4, the direct and reverse bifurcations are subcritical at $0 < \lambda < 0.1001$. There is a tiny region ($0.1001 < \lambda < 0.1015$) in which the direct bifurcation is supercritical, while the reverse one stays subcritical. At $\lambda \approx 0.1015$ the reverse bifurcation also switches to the supercritical type, making the loop completely convex. It keeps this shape up to the point of the disappearance of the loop, at $\lambda_{\max}^{(s=2)} \approx 0.1102$.

IV. THE LINEAR-STABILITY ANALYSIS

The stability of stationary solutions (2) was explored using the standard approach: we take a perturbed solution with

$$
\begin{aligned}
\psi(r, \theta, z) &= [U(r) + \delta U(r, \theta, z)] \exp(is\theta) \exp(ikz), \\
\phi(r, \theta, z) &= [V(r) + \delta V(r, \theta, z)] \exp(is\theta) \exp(ikz),
\end{aligned} \tag{6}
$$

where small perturbations are looked for, as usual, in the form of angular eigenmodes, with an integer azimuthal perturbation index, n, and the respective instability growth rate γ_n,

$$
\begin{aligned}
\delta U &= [U_+(r, z) \exp(in\theta) + U_-(r, z) \exp(-in\theta)] \exp(\gamma_n z), \\
\delta V &= [V_+(r, z) \exp(in\theta) + V_-(r, z) \exp(-in\theta)] \exp(\gamma_n z).
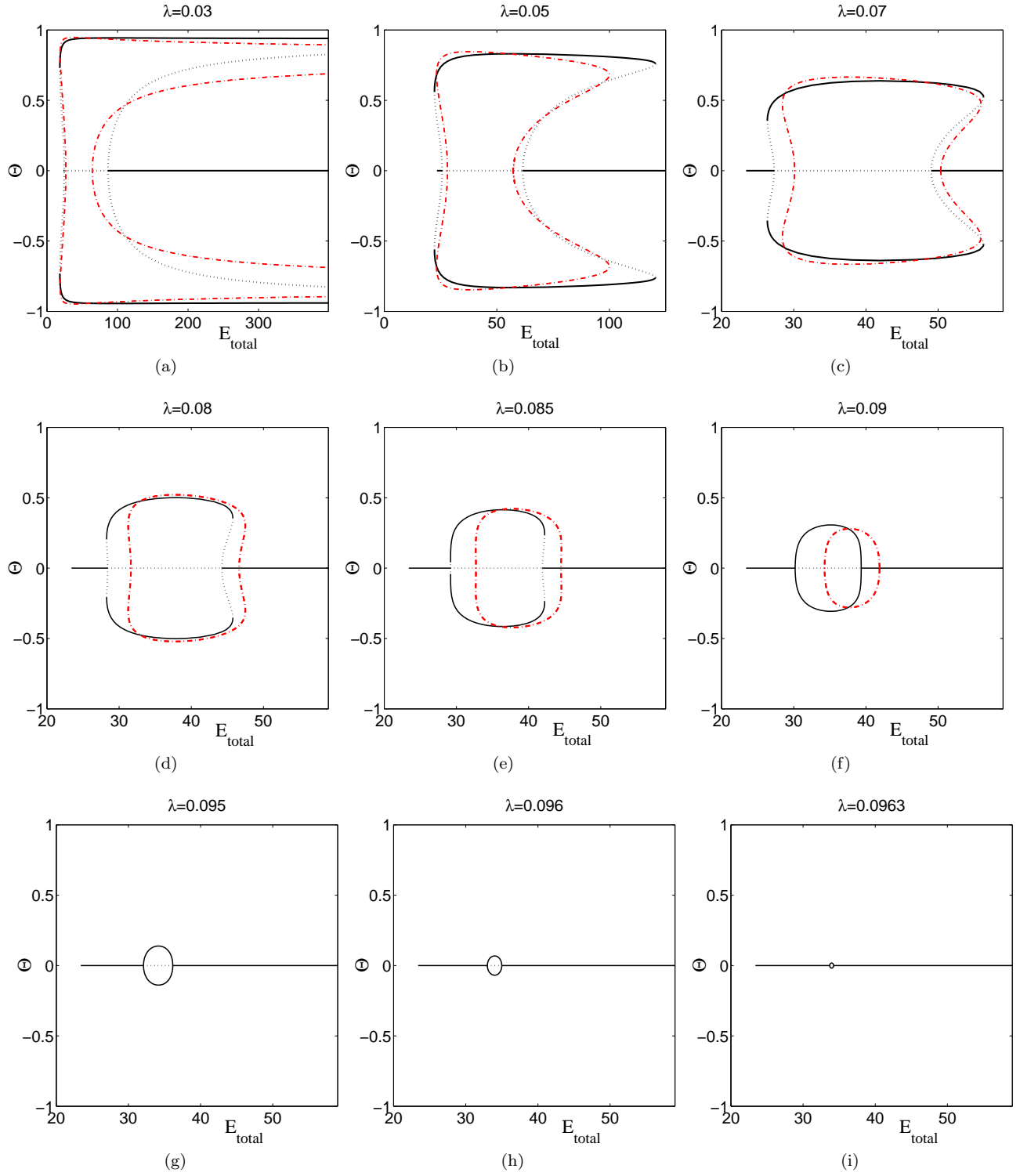\end{aligned} \tag{7}
$$

FIG. 2. (Color online) The bifurcation diagrams, in the $(E_{\text{total}}, \Theta)$ plane, for fundamental solitons ($s = 0$), at different values of the linear-coupling constant, λ. Here and in other bifurcation diagrams, stable and unstable branches are shown by solid and dotted lines, respectively (see also Fig. 5(a) below, for details of the stability of solution branches displayed in this figure). The bifurcation loops produced by the variational approximation (section V) are shown too, by dashed-dotted red curves.
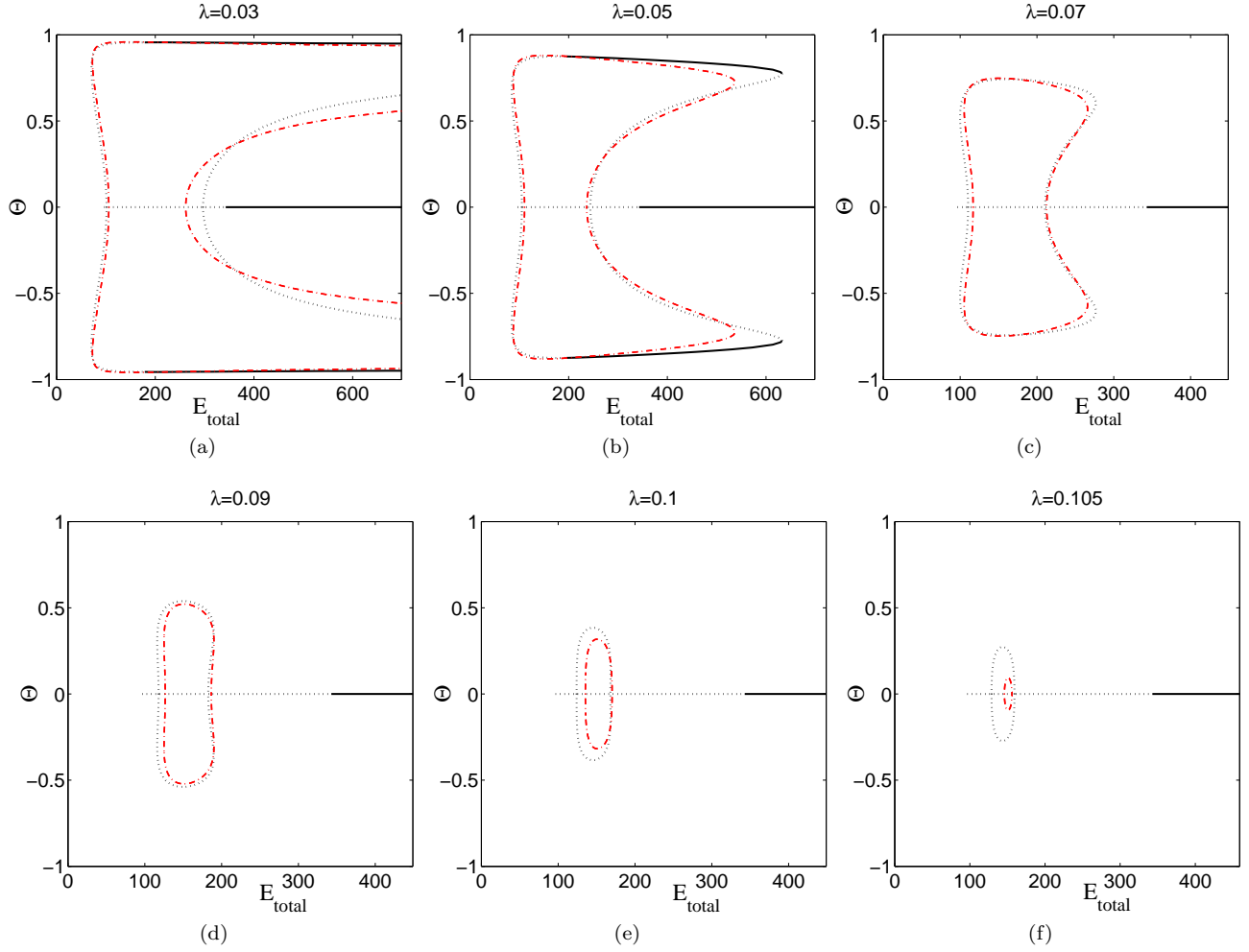
FIG. 3. (Color online) The same as in Fig. 2, but for vortex solitons with $s = 1$. See also Fig. 6(a) below for details of the stability.

Taking the perturbation in this form leads to a closed system of linearized equations generated by the substitution of expressions (6) and (7) into Eqs. (3):

$$-kU_+ + i\gamma_n U_+ + \frac{\partial^2 U_+}{\partial r^2} + \frac{1}{r}\frac{\partial U_+}{\partial r} - \frac{(s+n)^2}{r^2}U_+$$
$$+(2 - 3U^2)U^2 U_+ + (1 - 2U^2)U^2 U_-^* = -\lambda V_+;$$
$$-kU_- + i\gamma_n U_- + \frac{\partial^2 U_-}{\partial r^2} + \frac{1}{r}\frac{\partial U_-}{\partial r} - \frac{(s-n)^2}{r^2}U_-$$
$$+(2 - 3U^2)U^2 U_- + (1 - 2U^2)U^2 U_+^* = -\lambda V_-;$$
$$-kV_+ + i\gamma_n V_+ + \frac{\partial^2 V_+}{\partial r^2} + \frac{1}{r}\frac{\partial V_+}{\partial r} - \frac{(s+n)^2}{r^2}V_+$$
$$+(2 - 3V^2)V^2 V_+ + (1 - 2V^2)V^2 V_-^* = -\lambda U_+;$$
$$-kV_- + i\gamma_n V_- + \frac{\partial^2 V_-}{\partial r^2} + \frac{1}{r}\frac{\partial V_-}{\partial r} - \frac{(s-n)^2}{r^2}V_-$$
$$+(2 - 3V^2)V^2 V_- + (1 - 2V^2)V^2 V_+^* = -\lambda U_- .$$
(8)

These equations are to be solved with the boundary conditions, which demand $\{U_\pm, V_\pm\} \to r^{|s\pm n|}$ at $r \to 0$, and the exponential decay of the perturbation eigenmodes at $r \to \infty$.

There are several available numerical methods for solving such a boundary-value problem and finding the pertur-
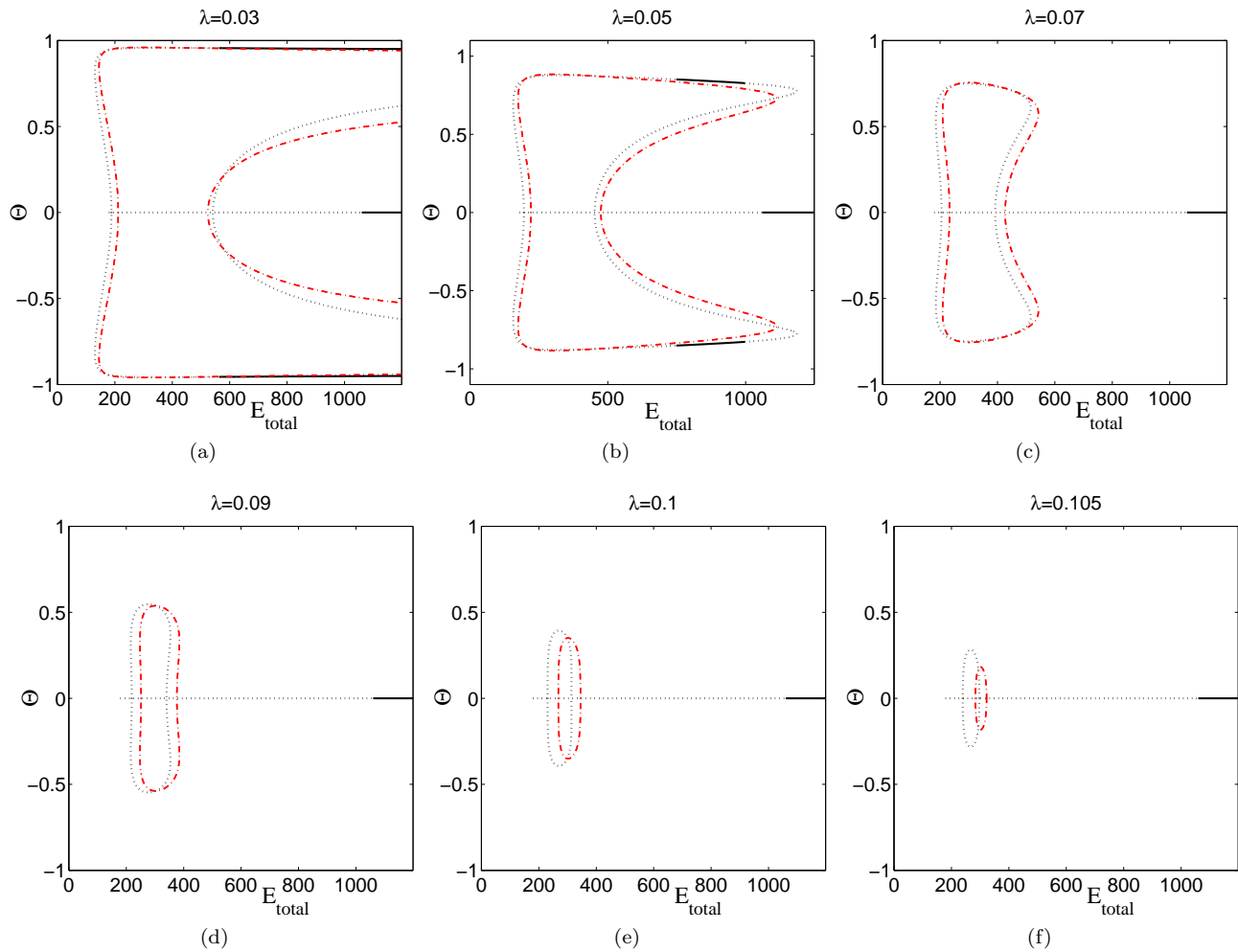
FIG. 4. (Color online) The same as in Figs. 2 and 3, but for vortex solitons with $s = 2$. See also Fig. 7(a) below for details of the stability.

bation growth rates, γ_n [5, 11, 26]. We treated Eqs. (8) as an algebraic eigenvalue problem for γ_n, and solved it directly, using a finite-difference method. The largest instability-growth rate was identified as the real part of the most unstable eigenvalue, $\max\{\text{Re}(\gamma_n)\}$. This approach has confirmed the azimuthal stability of the fundamental solitons ($s = 0$) and revealed instability regions for vortices with $s = 1, 2$.

For $s = 0$, the most dangerous perturbation azimuthal index is $n = 0$ (i.e., as said above, the fundamental solitons are not destabilized by azimuthal perturbations). An example of the ensuing curves which display the maximum growth rate, in the case corresponding to the bifurcation diagram that features the double bistability at $\lambda = 0.05$ (see Fig. 2), is shown in Fig. 5. As expected, unstable are backward-going portions of the asymmetric solution branches, i.e., in the region between the bifurcation points and turning points of the bifurcation curves. As might be expected too, the symmetric solutions are unstable in the entire region between the points of the direct and reverse bifurcations.

For vortices with $s = 1$, the growth-rate curves pertaining to $n = 0$ feature the same behavior as for the fundamental solitons. However, additional unstable eigenmodes, for both the symmetric and asymmetric solutions, were found with azimuthal indices $n = 1, 2, 3$. On the other hand, no unstable perturbations were detected for larger $n > 3$. A typical example displaying all the existing unstable eigenvalues for $s = 1$ is presented in Fig. 6, for the same coupling constant as in Fig. 5, $\lambda = 0.05$. In particular, panel (d) in this figure shows the results for the symmetric solutions. The eigenmode that remains the last unstable one with the increase of E_{total} pertains to $n = 2$. This instability ceases when the energy attains value $E_{\text{total}} \approx 340$, which corresponds to propagation constant $k \approx 0.2$. This value is exactly the expected one, according to relation $k^{(\text{sta})} \approx 0.15 + \lambda$, where $k \approx 0.15$ is the known stability threshold in the single-component model ($\lambda = 0$), for $s = 1$ [16]. Further, the results for unstable eigenmodes disturbing the two inner asymmetric branches (the portions of the branches that commence at the bifurcation point and end at the
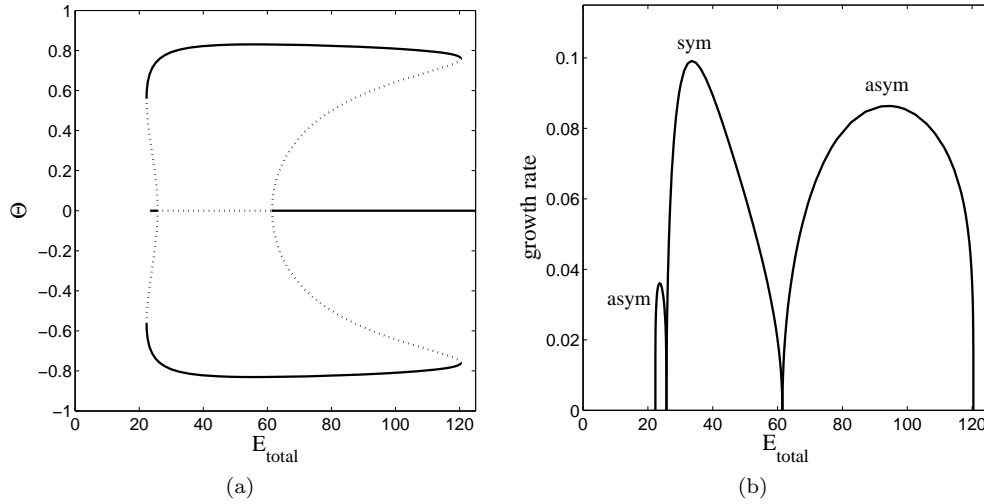
FIG. 5. (a) The bifurcation diagram, for the fundamental solitons ($s = 0$) at $\lambda = 0.05$, cf. Fig. 2. (b) The corresponding maximum growth rate of perturbation eigenmodes for the symmetric and asymmetric solutions.

turning points) are shown in panel 6(c). At the respective edge points, these curves are linked to their counterparts (continuations) in panels 6(d) and 6(b), the latter panel pertaining to the outer asymmetric branches. The conclusion is that the inner portions are completely unstable (as well as in the case of $s = 0$, cf. Fig. 5), while parts of the outer branches are *stable*. In the case shown in Fig. 6 (recall it pertains to $\lambda = 0.05$), the stability segment of the outer branch of the asymmetric solutions with $s = 1$ is $195 < E_{\text{total}} < 630$, which corresponds to $0.165 < k < 0.186$.

With the increase of λ, the stable section of the asymmetric branch with $s = 1$ shrinks, and it disappears at $\lambda \approx 0.067$ (which still corresponds to the double-concave shape of the loop with both the direct and reverse bifurcations of the subcritical type). At larger values of λ, the instability accounted for by the perturbation mode with $n = 2$ covers the entire asymmetric branch. With the further increase of λ, the instability regions corresponding to the eigenmodes with the other values of n also expand and gradually cover the entire asymmetric branch. In all the cases that we have examined, the growth rate corresponding to $n = 2$ is always the largest one for the upper asymmetric branch.

In the case of the double vortex, with $s = 2$, results of the stability analysis are presented in Fig. 7, again for $\lambda = 0.05$. As in the case of $s = 1$, the eigenmode that determines the stability boundaries has $n = 2$. However, in this case the growth rate for perturbations with $n = 2$ is not necessarily the highest for the outer asymmetric branch, and the azimuthal index of the dominant perturbation eigenmode switches from $n = 4$ to $n = 3$ and then to $n = 2$. Similar to the behavior of the vortex with $s = 1$, the stability region of the asymmetric stable solutions diminishes with the increase of λ. The entire diagram is totally unstable for $\lambda > 0.0505$, which is slightly larger than $\lambda = 0.05$ for which Fig. 7 is displayed. As well as in the case of $s = 1$, the ultimate destabilization occurs when the shape of the bifurcation loop is still double-concave.

Finally, the symmetric vortices with $s = 2$ are unstable at $\lambda < k < 0.162 + \lambda$, where $k \approx 0.162$ is the stability threshold for $s = 2$ in the single-component model [16]. This threshold corresponds to the total energy $E \approx 1060$ of the symmetric vortex.

V.   THE VARIATIONAL ANALYSIS

The stationary solutions can also be studied analytically by means of the variational approximation (VA), cf. Ref. [20], taking into regard that stationary equations (3) can be derived from the Lagrangian,

$$\frac{L}{\pi} = \int_0^\infty r \left\{ -k(U^2 + V^2) - \left[\left(\frac{dU}{dr}\right)^2 + \left(\frac{dV}{dr}\right)^2 \right] - \frac{s^2}{r^2}(U^2 + V^2) \right.$$
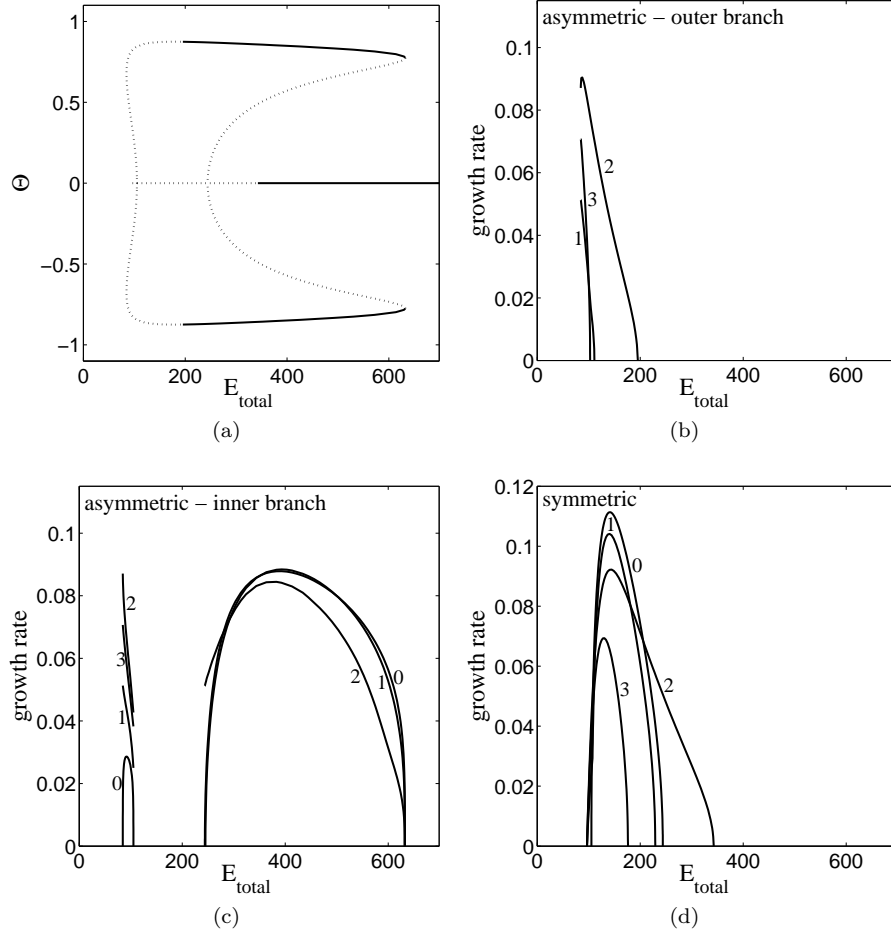$$\left. + \frac{1}{2}(U^4 + V^4) - \frac{1}{3}(U^6 + V^6) - 2\lambda UV \right\} dr. \tag{9}$$

FIG. 6. (a) The bifurcation diagram for the vortices with $s = 1$ at $\lambda = 0.05$, cf. Fig. 3. The corresponding maximum growth rates of perturbation eigenmodes for the inner and outer asymmetric branches and the symmetric one are shown in panels (b), (c), and (d), respectively. The labels near the curves indicate the mode's azimuthal number. Note that the plots which appear aborted in panels (b) and (c) are actually continuations of each other and of the plots in panel (d). This is in accordance with the fact that the outer and inner branches of the asymmetric states are linked at the turning points of the bifurcation diagram, and the symmetric and inner asymmetric branches are linked at the bifurcation points.

To approximate solutions to Eqs. (3) (generally, asymmetric ones), the following *ansatz* was adopted, with common width W of both components, but different amplitudes, A and B:

$$\{U(r), V(r)\}_{\text{ansatz}} = \{A, B\}r^s \exp\left(-\frac{r^2}{2W^2}\right), \tag{10}$$

where $s = 0, 1, 2$ is the same spin as above. The energies of the two components of this ansatz, defined according to (4), are

$$\{E_{U,V}\}_{\text{ansatz}} = \pi s! \{A^2, B^2\} W^{2(s+1)} \tag{11}$$

The substitution of the ansatz into Lagrangian (9) and the integration yield the effective Lagrangian:

$$\frac{2}{\pi}L_{\text{eff}} = -s!k(A^2 + B^2)W^{2(1+s)} - (s+1)s!(A^2 + B^2)W^{2s}$$

$$+ \frac{(2s)!}{2^{2(1+s)}}(A^4 + B^4)W^{2(1+2s)} - \frac{(3s)!}{3^{3s+2}}(A^6 + B^6)W^{2(1+3s)} + 2s!\lambda ABW^{2(1+s)}. \tag{12}$$

It is convenient to redefine the variational parameters as

$$\alpha \equiv \left(W^2/\sqrt{2}\right)(A + B), \ \beta \equiv \left(W^2/\sqrt{2}\right)(A - B),$$
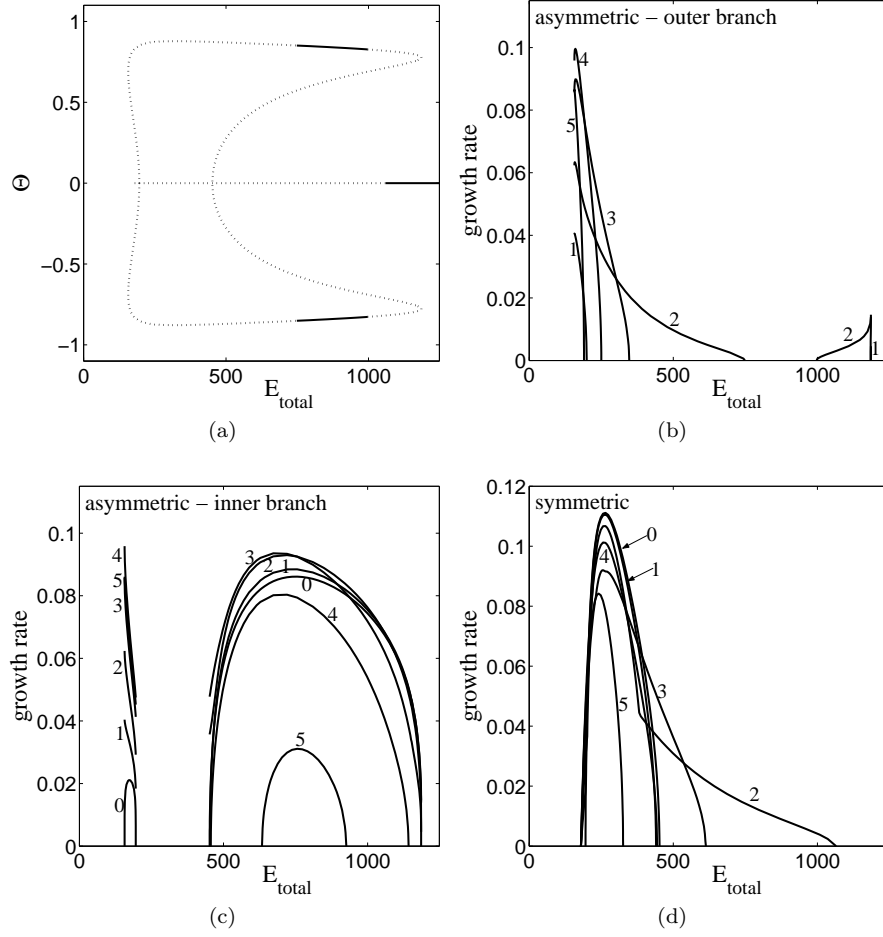
FIG. 7. The same as in Fig. 6, but for the double vortices ($s = 2$) at $\lambda = 0.05$.

in terms of which effective Lagrangian (12) takes the form of

$$\frac{2}{\pi}L_{\text{eff}} = -(s+1)s!(\alpha^2 + \beta^2) + \left[-s!k(\alpha^2 + \beta^2) + \frac{(2s)!}{2^{2s+3}}(\alpha^4 + \beta^4 + 6\alpha^2\beta^2) \right.$$

$$\left. -\frac{(3s)!}{4 \cdot 3^{3s+2}}(\alpha^6 + \beta^6 + 15\alpha^4\beta^2 + 15\alpha^2\beta^4) + s!\lambda(\alpha^2 - \beta^2) \right] W^2. \tag{13}$$

Values of the variational parameters corresponding to stationary solutions, α, β and W, are determined by the Euler-Lagrange equations, $\partial L_{\text{eff}}/\partial(W^2) = \partial L_{\text{eff}}/\partial(\alpha^2) = \partial L_{\text{eff}}/\partial(\beta^2) = 0$, i.e.,

$$-k(\alpha^2 + \beta^2) + \frac{(2s)!}{2^{2s+3}s!}(\alpha^4 + \beta^4 + 6\alpha^2\beta^2)$$

$$-\frac{(3s)!}{4 \cdot 3^{3s+2}s!}(\alpha^6 + \beta^6 + 15\alpha^4\beta^2 + 15\alpha^2\beta^4) + \lambda(\alpha^2 - \beta^2) = 0, \tag{14}$$

$$-kW^2 - (s+1) + \frac{(2s)!}{2^{2s+2}s!}(\alpha^2 + 3\beta^2)W^2$$

$$-\frac{(3s)!}{4 \cdot 3^{3s+1}s!}(\alpha^4 + 10\alpha^2\beta^2 + 5\beta^4)W^2 + \lambda W^2 = 0, \tag{15}$$

$$-kW^2 - (s+1) + \frac{(2s)!}{2^{2s+2}s!}(\beta^2 + 3\alpha^2)W^2$$

$$-\frac{(3s)!}{4 \cdot 3^{3s+1}s!}(\beta^4 + 10\alpha^2\beta^2 + 5\alpha^4)W^2 - \lambda W^2 = 0. \tag{16}$$

The variational solutions are obtained by numerically solving the system of equations, (14)-(16) for α, β and W, for given s, λ and k. In this way, several VA-predicted bifurcation loops were constructed, for different values of λ and for $s = 0, 1$ and 2, as shown above in Figs. 2, 3 and 4 by dashed-dotted curves, alongside the numerically found loops. The figures show that the VA quite accurately predicts the transformation of the bifurcation loop from the concave shape to the convex one with the increase of λ. An adequate indication of the accuracy of the VA is given by comparing critical values of λ at which the symmetry-breaking bifurcations disappear, along with the bifurcation loops. For that purpose, we set $\beta = 0$ in Eqs. (14)-(16) and subtract the second equation from the third, which yields

$$\alpha^2 = \frac{3^{3s+1}s!}{(3s)!}\left(\frac{(2s)!}{2^{2s+2}s!} \pm \sqrt{\left(\frac{(2s)!}{2^{2s+2}s!}\right)^2 - 2\frac{(3s)!}{3^{3s+1}s!}\lambda}\right). \tag{17}$$

Within the framework of of the VA, the asymmetric solutions exist under the condition that expression (17) yields real values:

$$\lambda < \lambda_s \equiv \frac{3^{3s+1}((2s)!)^2}{2^{4s+5}(3s)!s!}. \tag{18}$$

For $s = 0, 1$ and 2, Eq. (18) predicts critical values $\lambda_0 = 0.09375$, $\lambda_1 = 0.10547$, and $\lambda_2 = 0.10679$. The comparison with their numerically found counterparts shows that the difference is 2.8%, 4.3% and 3.9%, respectively.

To calculate coordinates of the VA-predicted bifurcation points, we substitute expression (17) into Eq. (16) with $\beta = 0$. Both the variational and the numerically generated plots for values of E and k at the bifurcation points are shown, versus the coupling constant, λ, in Fig. 8. It is seen that the variational and numerical results are always in good agreement for the direct bifurcation. On the other hand, the approximation for the reverse bifurcation becomes inaccurate for very small values of λ. This difference is explained by the fact that, near the reverse bifurcation, the actual profiles of the soliton components become increasingly rectangular-like, i.e., different from the shape assumed by ansatz (10).

VI.   DEVELOPMENT OF THE INSTABILITY OF VORTEX RINGS

To explore results of the instability development, direct simulations of Eqs. (1) were performed by means of the standard pseudospectral split-step method, for initial conditions corresponding to the stationary solutions presented in section III. Perturbations were not explicitly added to unstable solitons, the instability being initiated by truncation errors of the numerical code. First, we demonstrate the splitting of vortex solitons which are unstable against azimuthal perturbations. For the single-component model, a similar numerical analysis was reported in Ref. [16], where it was concluded that, generally, the azimuthal index, n, of the most unstable eigenmode determines the number of fragments produced by the splitting.

Figure 9 displays the numerically simulated evolution of the asymmetric vortex ring with $s = 1$, $\lambda = 0.05$, $k = 0.155$ and $E_{\text{total}} \approx 150$, for which the single unstable perturbation eigenmode has $n = 2$, as per Fig. 6(b). In this case, the breakup of the vortex becomes conspicuous at $z_{\text{split}} \approx 900$, giving rise to two fragments, in accordance with the linear-stability analysis.

Similar results for the double asymmetric vortices ($s = 2$) and $\lambda = 0.05$ are presented in Figs. 10–12. The initial states were chosen so as to have, in each case, the largest growth rate at a different value of n. To this end, we took $k = 0.112$, 0.1505, 0.174, which correspond to the vortices with $E_{\text{total}} \approx 165$, 250, 500, the corresponding largest instability growth rates being $\gamma_{n=4} \approx 0.098, \gamma_{n=3} \approx 0.047, \gamma_{n=2} \approx 0.009$, respectively. As expected, the numbers of fragments generated by the breakup are consistent with these values of n. We stress that, in all the cases presented here, there is a well-pronounced dominant eigenmode. As mentioned in Ref. [16], when the parameters are taken close to borders between regions dominated by unstable eigenmodes with different azimuthal indices n, it is difficult to predict which one will determine the outcome of the splitting.

Values of the propagation distance needed for the splitting to commence are also in agreement with the predictions based on the growth rates of the linear instability. In particular, a large growth rate was found for $k = 0.112$ ($E_{\text{total}} \approx 165$) and, accordingly, in that case the splitting starts very early, at $z_{\text{split}} \approx 170$. For $k = 0.1505$ ($E_{\text{total}} \approx 250$), the breakup starts later, at $z_{\text{split}} \approx 680$, and when the growth rate is small – for instance, at $k = 0.174$ ($E_{\text{total}} \approx 500$) – the splitting sets in after a very long evolution, at $z_{\text{split}} \approx 3250$. In all the cases that we have examined, the fragments maintain the asymmetry of the original unstable vortex rings.

Note that unstable asymmetric solutions could transform into stable symmetric ones (and vise versa) if the only unstable perturbation eigenmode were the one with $n = 0$. In fact, this happens solely for $s = 0$ (see Fig. 5, for example). In all the cases that we have examined, the azimuthal instability of the vortices with $s = 1$ and 2 destabilizes
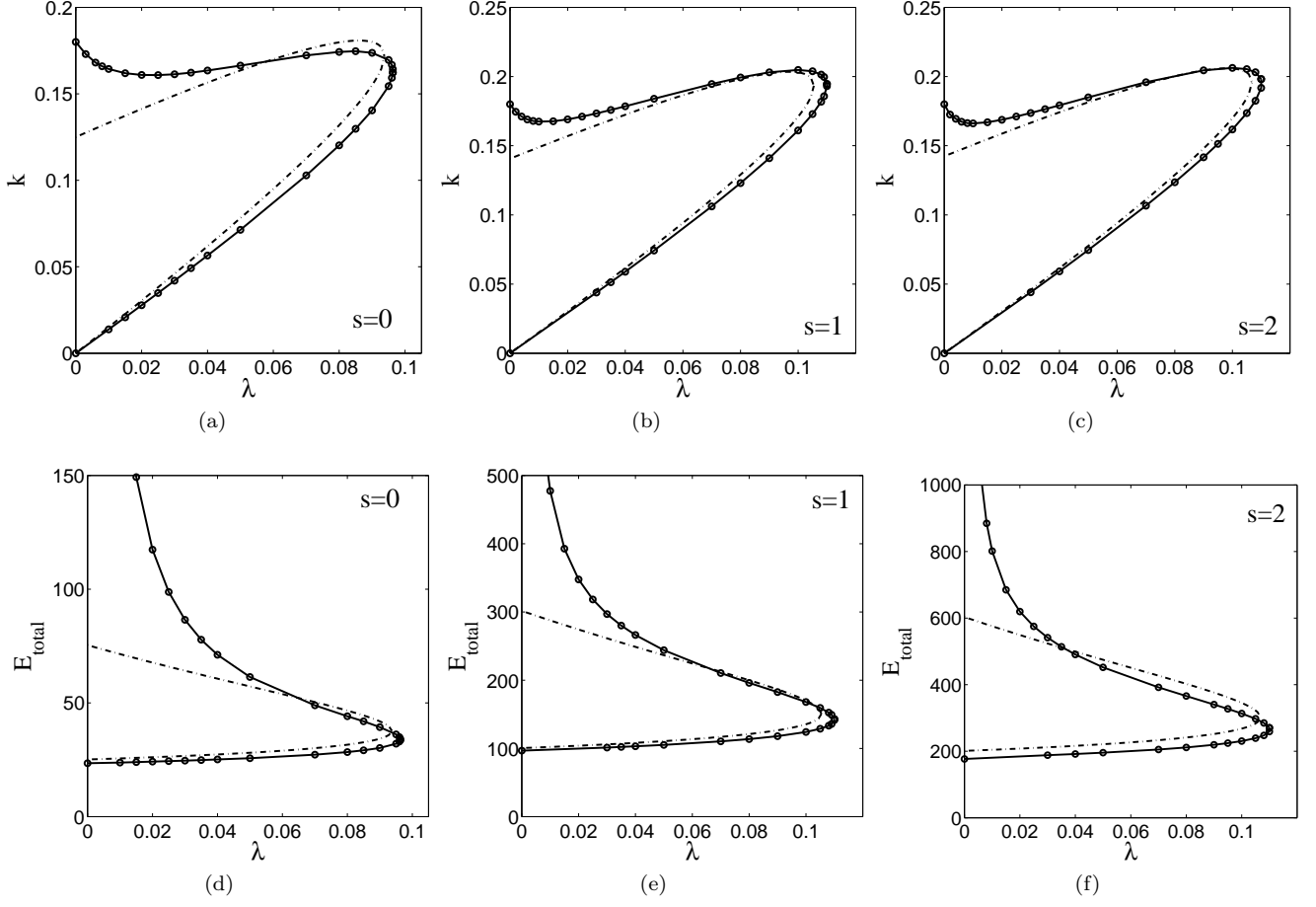
FIG. 8. The comparison of the numerically generated (circles connected by continues lines) and variationally predicted (dashed-dotted lines) points of the direct and reverse bifurcations. (a)-(c) The propagation constant, k, at which the bifurcations occur, as a function of λ, for $s = 0, 1$ and 2. (d)-(f) The same for the total energy, E_{total}.

and destroys the solutions, before they could be reshaped into stable symmetric or asymmetric structures with the same s.

VII. INTERACTIONS BETWEEN SOLITONS

Direct simulations were also used to study interactions between two initially quiescent solitons separated by a relatively small distance. In the 2D single-component model, a similar investigation was reported in Ref. [14], for vortices with $s = 1$. Collisions between asymmetric solitons in the 1D dual-core model were studied earlier in Ref. [29]. Here we focus on pairs of initially quiescent solitons (rather than moving ones), as the interaction effects are strongest in such a case.

Our analysis was performed for several combinations of stable asymmetric solutions, for all the three values of the spin considered here, $s = 0, 1, 2$. First, we examined the interaction between identical solitons separated by distance Δx, namely: $\{U, V\}_{\text{initial}}(x, y) = \{U, V\}_{\text{stationary}}(x - \Delta x, y) + \{U, V\}_{\text{stationary}}(x + \Delta x, y)$. Next, we considered pairs of cross-identical asymmetric solitons (one being a specular counterpart of the other): $\{U, V\}_{\text{initial}}(x, y) = \{U, V\}_{\text{stationary}}(x - \Delta x, y) + \{V, U\}_{\text{stationary}}(x + \Delta x, y)$. We have also performed the simulations for the soliton pairs with the phase shift of $\Delta \theta = \pi$.

The results are presented in Figs. 13–16. In accordance with the known principle [30], we observed that identical solitons with even values of the spin, $s = 0$ or $s = 2$, attract each other in the in-phase configuration, while the vortices with $s = 1$ exhibit the attraction when they are *out-of-phase*, with $\Delta \theta = \pi$. The attraction results in inelastic collisions, as seen in Figs. 13(a)–(b), 16(a)–(b), and 15(a)–(b). If both solitons are fundamental ones, the inelastic interaction ends up with their merger into a single pulse (which is not necessarily another stationary fundamental
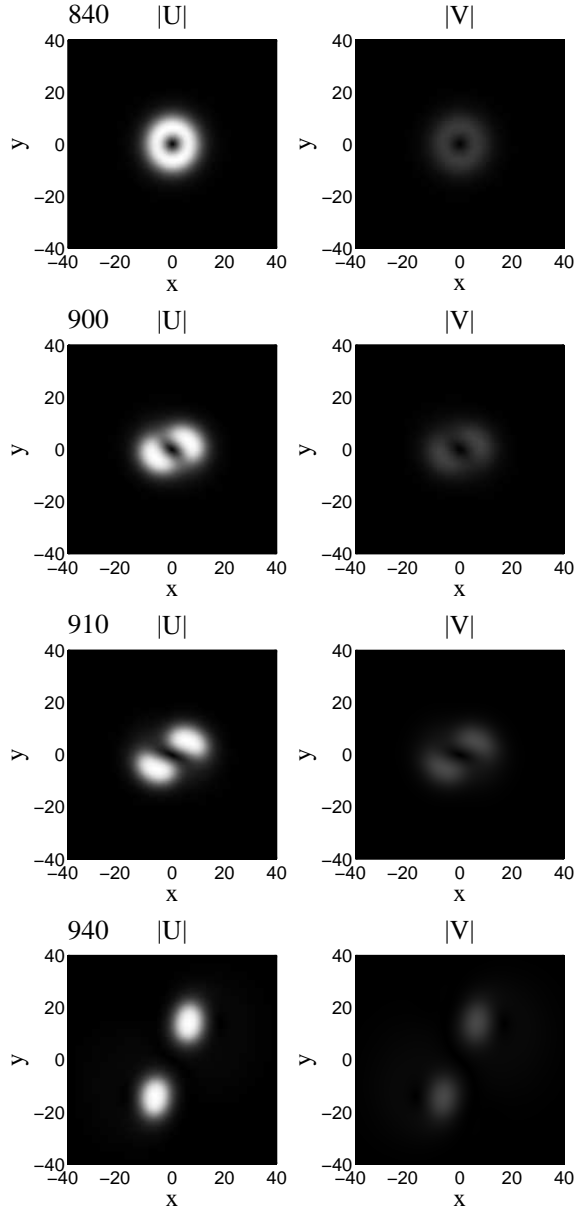
FIG. 9. Gray-scale plots illustrating the splitting of an unstable vortex solution, at $s = 1$ and $k = 0.155$ ($E_{total} \approx 150$). Values of the propagation distance are labeled above the left frames.
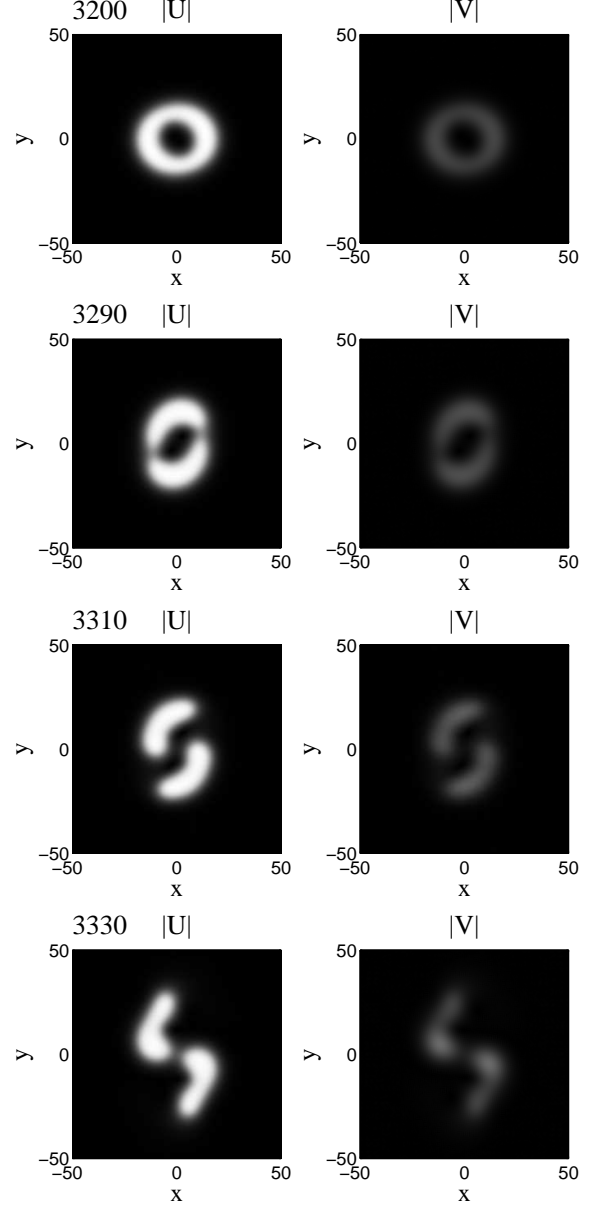

FIG. 10. The same as in Fig. 9, but for $s = 2$ and $k = 0.174$ ($E_{total} \approx 500$).

soliton). If vortex rings are involved into the collision, the eventual result is destruction of the ring(s), and formation of a disordered pattern.

On the other hand, repulsion is observed, also in agreement with the predictions of Ref. [30], between out-of-phase solitons ($\Delta\theta = \pi$) with even values of the spin, $s = 0$ and 2 (not shown here in detail), and between *in-phase* vortices with $s = 1$. In the case of the repulsion, the interactions produce, as a matter of fact, no visible effect, leading only to a small increase of the separation between the two solitons, as shown, for $s = 1$, in Fig 14(a)–(b).

Additional simulations were carried out for soliton pairs with different spins. Figure 17 shows a typical example for an in-phase vortex pair with $s = 1$ and $s = 2$. In this case, the phase varies smoothly between the centers of the two vortices, similar to the case of the in-phase pairs with $s = 0$ or $s = 2$, and the out-of-phase one with $s = 1$. Accordingly, the simulations demonstrate a strong attractive interaction in this case. On the other hand, for the same pair with $s = 1$, $s = 2$ and $\Delta\theta = \pi$, the change of the phase between the vortices is very steep, similar to the situations when the solitons with equal spins repel each other, and, accordingly, the vortices under consideration repel
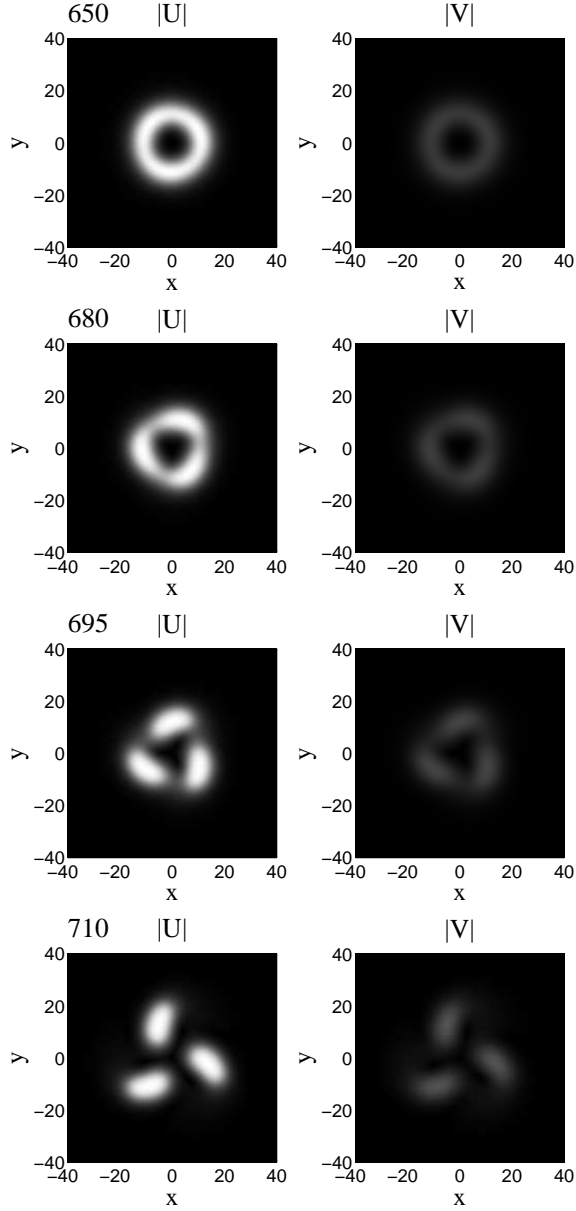
FIG. 11. The same as in Figs. 9 and 10, but for $s = 2$ and $k = 0.1505$ ($E_{total} \approx 250$).
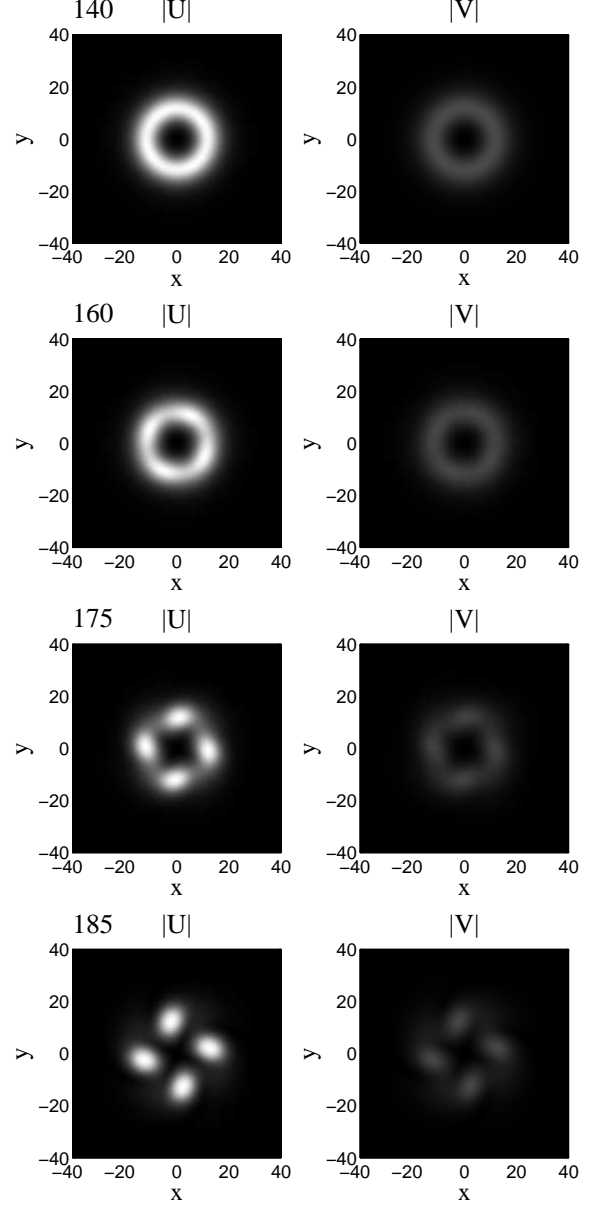
FIG. 12. The same as in Figs. 9–11, but for $s = 2$ and $k = 0.112$ ($E_{total} \approx 165$).

each other too, which results in slow separation between the vortices (not shown here).

We have also studied the interaction between the vortex with $s = 1$ and the fundamental soliton ($s = 0$). In this case, an inelastic collision is observed in Fig. 18 for $\Delta\theta = \pi$, while for $\Delta\theta = 0$ the interaction is repulsive, producing no conspicuous effect (not shown here). These outcomes may be explained by the same character of the phase pattern between the solitons as above, i.e., smooth in the configuration leading to the attraction and strong interaction, and steep in the opposite case of the repulsion.

Interactions between stable symmetric solutions have also been examined, demonstrating results identical to those originally reported in Ref. [14] (not shown here). In particular, in this case the collisions maintain the symmetry between the two components, and do not lead to the appearance of any asymmetric final states.
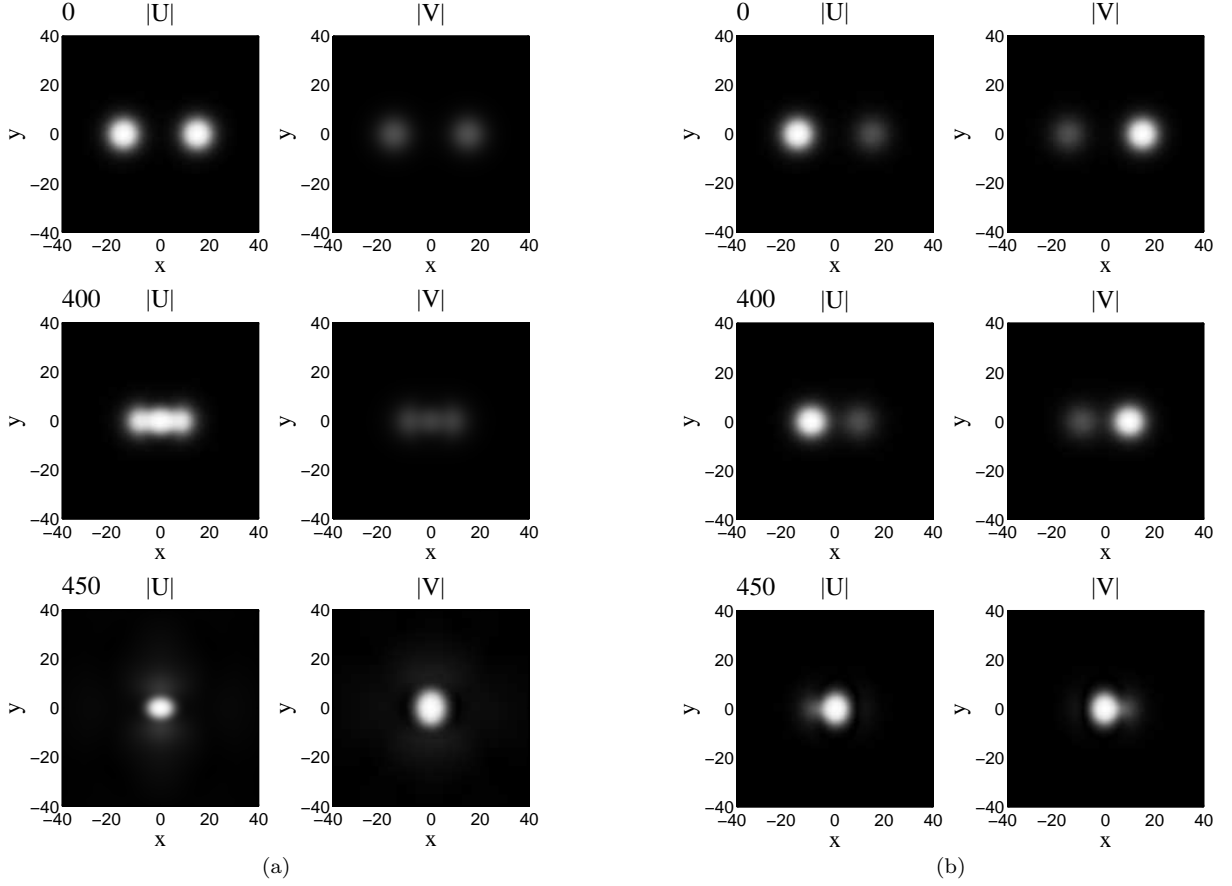
FIG. 13. The interaction between fundamental $(s = 0)$ in-phase $(\Delta\theta = 0)$ asymmetric solitons, with $\lambda = 0.05$, $k = 0.16$, and initial separation $\Delta x = 30$. In panel (a) the solitons are identical, while in (b) they are cross-symmetric. The evolution distances, z, are marked above each frame.

VIII. CONCLUSION

We have introduced a model of a 2D dual-core waveguide with the CQ (cubic-quintic) nonlinearity inside each core and the linear coupling between them. Families of fundamental $(s = 0)$ and vortical solitons, with spins $s = 1$ and 2, have been constructed, and their stability has been investigated. The model may be realized as a dual-core planar optical waveguide, or as a set of two tunnel-coupled parallel pancake-shaped traps for BEC. In the former case, the solitons are "planar light bullets". In particular, vortex solitons may be interpreted as a new species of the "bullets", *viz.*, spatiotemporal vortices.

The main objective of the work was to study symmetry-breaking bifurcations of the 2D solitons, both fundamental and vortical ones. If the inter-core coupling constant, λ, is not too large, the bifurcation diagrams for the solitons of all the types form closed loops, which connect points of direct and reverse bifurcations. The stability of all the solutions was investigated via the calculation of the corresponding eigenvalues for infinitely small perturbations around the solitons. In particular, it was found that, at sufficiently small values of λ, the loop for the fundamental solitons $(s = 0)$ includes two bistability regions, which may be of interest for potential applications, such as all-optical switching. This is also a new feature of the loop in comparison with its earlier studied counterpart in the 1D version of the model, which could feature a single bistability domain. At larger values of λ, both bistable regions vanish and the loop's shape becomes plainly convex. With the further increase of λ, the loop shrinks to zilch and disappears, leaving only stable symmetric solitons. The vortical solitons may be easily destabilized by azimuthal perturbations, but they also have stability regions, as long as the corresponding bifurcation loop keeps its double-concave shape. We have also developed a quasi-analytical approach to the description of the bifurcation diagrams, based on the variational approximation, which produces reasonably accurate predictions, in comparison with the numerical results.

In direct simulations, we have demonstrated the splitting of azimuthally unstable asymmetric solitons into sets of fragments. The number of the fragments usually corresponds to the azimuthal index of the most unstable eigenmode
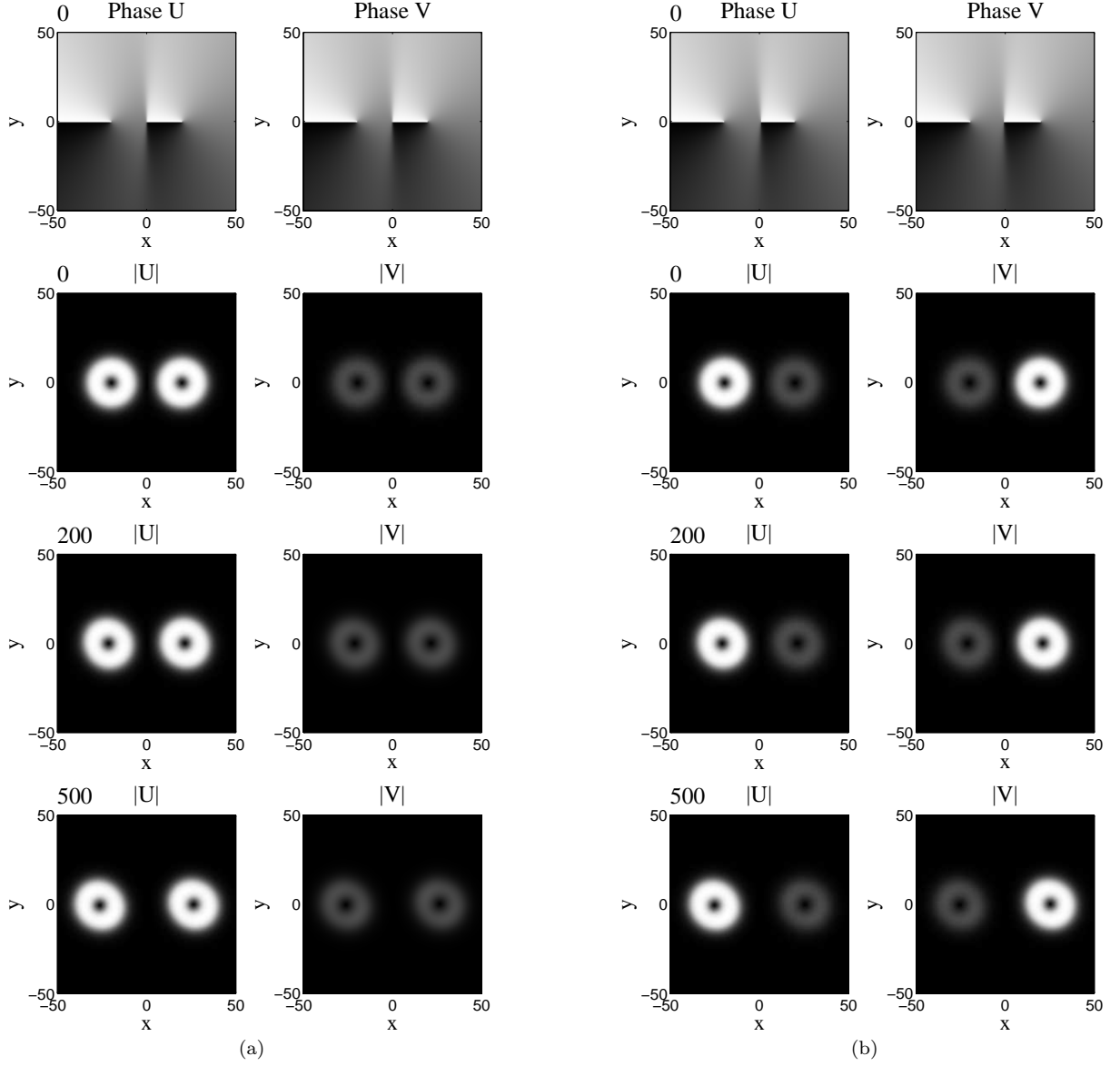
FIG. 14. The interaction between asymmetric in-phase vortices with $s = 1$, $\lambda = 0.05$, $k = 0.18$, and $\Delta x = 40$. Notice the *repulsion* between the in-phase vortex solitons in this case.

of small perturbations. We have also studied interactions between initially quiescent solitons, and confirmed the earlier prediction [30], which states that the usual attractive/repulsive sign of the interaction between the in-phase/π-out-of-phase solitons with even values of the spin ($s = 0$ or 2), is reversed for the odd spin ($s = 1$). In the case of the attraction, the vortex solitons merge into disordered patterns, losing the initial topological structure.

This work may be naturally extended in other directions. In particular, it may be interesting to study symmetry-breaking effects in two-component 2D solitons and vortices in the system of NLSEs coupled by both linear and nonlinear terms, which may describe the co-propagation of two polarizations of light in a single nonlinear waveguide [1]. Moreover, the latter version of the model is meaningful in the 3D geometry too. Another relevant generalization still pertains to the dual-core waveguide, with the linear coupling between the two waves, while the competing nonlinear terms are quadratic and cubic, rather than cubic and quintic, cf. Ref. [31] and references therein. In that case, one may also expect bifurcation loops accounting for the breaking and restoration of the symmetry of two-component solitons.

[1] Yu. S. Kivshar and G. P. Agrawal, *Optical Solitons: From Fibers to Photonic Crystals* (Academic Press: San Diego, 2003).

[2] B. A. Malomed, D. Mihalache, F. Wise and L. Torner, *Spatiotemporal optical solitons*, J. Opt. B: Quant. Semicl. Opt. **7** (2005) R53.

[3] B. Gross and J. T. Manassah, Opt. Commun. **129** (1996) 143; L. Bergé, Phys. Rep. **303** (1998) 259.

[4] J. T. Manassah, P. L. Baldeck and R. R. Alfano, Opt. Lett. **13** (1988) 1090; J. T. Manassah *ibid.* **16** (1991) 563.

[5] R. H. Enns, D. E. Edmundson, S. S. Rangnekar and A. E. Kaplan, Opt. Quantum Electron. **24** (1992) S1295; R. McLeod, K. Wagner and S. Blair, Phys. Rev. A **52** (1995) 3254; J. T. Manassah and B. Gross, Laser Phys. **7** (1997) 9; D. E. Edmundson, Phys. Rev. E **55** (1997) 7636.

[6] A. A. Kanashov and A. M. Rubenchik, Physica **4D** (1981) 122; A. B. Blagoeva, S. G. Dinev, A. A. Dreischuh, and A. Naidenov, IEEE J. Quantum Electron. **QE-27** (1991) 2060.

[7] K. Hayata and M. Koshiba, Phys. Rev. Lett. **71** (1993) 3275; B. A. Malomed, P. Drummond, H. He, D. Anderson, A. Berntson and M. Lisak, Phys. Rev. E **56** (1997) 4725; D. V. Skryabin and W. J. Firth, Opt. Commun. **148** (1998) 79; D. Mihalache, D. Mazilu, B.A. Malomed and L. Torner, *ibid.* **152** (1998) 365; D. Mihalache, D. Mazilu, J. Dörring and L. Torner, *ibid.* **159** (1999) 129; D. Mihalache, D. Mazilu, L. -C. Crasovan, L. Torner, B. A. Malomed and. F. Lederer, Phys. Rev. E **62** (2000) 7340.

[8] M. Quiroga-Teixeiro, A. Berntson and H. Michinel, J. Opt. Soc. Am. B **16** (1999) 1697.

[9] A. Desyatnikov, A. Maimistov, B. Malomed, Phys. Rev. E **61** (2000) 3107.

[10] X. Liu, L. J. Qian and F. W. Wise, Phys. Rev. Lett. **82** (1999) 4631; X. Liu, K. Beckwitt and F. W. Wise, Phys. Rev. E **61** (2000) R4722.

[11] L. Torner and D. V. Petrov, Electron. Lett. **33** (1997) 608; D. V. Petrov, L. Torner, Opt. Quant. Electron. **29** (1997) 1037; W. J. Firth and D. V. Skryabin, Phys. Rev. Lett. **79** (1997) 2450; D. V. Skryabin, W. J. Firth, Phys. Rev. E **58** (1998) 3916.

[12] D. V. Petrov , L. Torner, J. Martorell, R. Vilaseca, J. P. Torres and C. Cojocaru, Opt. Lett. **23** (1998) 1444.

[13] I. Towers, A. V. Buryak, R. A. Sammut and B. A. Malomed, Phys. Rev. E **63** (2001) 055601(R).

[14] M. Quiroga-Teixeiro and H. Michinel, J. Opt. Soc. Am. B **14** (1997) 2004.

[15] I. Towers, A. V. Buryak, R. A. Sammut, B.A. Malomed, L.-C. Crasovan, and D. Mihalache, Phys. Lett. A **288** (2001) 292; B.A. Malomed, G. D. Peng, P. L. Chu, I. Towers, A. V. Buryak, and R. A. Sammut, Pramana **57** (2001) 1061.

[16] L.-C. Crasovan, B. A. Malomed and D. Mihalache, Pramana **57** (2001) 1041; B.A. Malomed, L.-C. Crasovan and D. Mihalache, Physica D **161** (2002) 187.

[17] R. L. Pego and H. A. Warchall, J. Nonlinear Sci. **12** (2002) 347.

[18] L. Pitaevskii and S. Stringari, *Bose-Einstein Condensation* (Clarendon Press: Oxford, 2003).

[19] L. Albuch, B. A. Malomed, Mathematics and Computers in Simulation **74** (2007) 312; Z. Birnbaum and B. A. Malomed, Physica D **237** (2008) 3252.

[20] A. Gubeskys and B. A. Malomed, Phys. Rev. A **76** (2007) 043623.

[21] F. K. Abdullaev, A. Gammal, L. Tomio and T. Frederico, Phys. Rev. A **63** (2001) 043604; F. K. Abdullaev and M. Salerno, *ibid.* A **72** (2005) 033617.

[22] G. S. Agarwal and S. Dutta Gupta, Phys. Rev. A **38** (1988) 5678; K. Dolgaleva, R. W. Boyd and J. E. Sipe, *ibid.* A **76** (2007) 063806.

[23] F. Smektala, C. Quemard, V. Couderc, A. Barthélémy and J. Non-Cryst. Solids **274** (2000) 232; K. Ogusu, J. Yamasaki, S. Maeda, M. Kitao and M. Minakata, Opt. Lett. **29** (2004) 265; C. Zhan, D. Zhang, D. Zhu, D. Wang, Y. Li, D. Li, Z. Lu, L. Zhao and Y. Nie, J. Opt. Soc. Am. B **19** (2002) 369; G. Boudebs, S. Cherukulappurath, H. Leblond, J. Troles, F. Smektala and F. Sanchez, Opt. Commun. **219** (2003) 427; R. A. Ganeev, M. Baba, M. Morita, A. I. Ryasnyansky, M. Suzuki, M. Turu and H. Kuroda, J. Opt. A: Pure Appl. Opt. **6** (2004) 282; E. L. Falcão-Filho, C. B. de Araújo and J. J. Rodrigues Jr., J. Opt. Soc. Am. B **24** (2007) 2948.

[24] D. Neshev, T. J. Alexander, E. A. Ostrovskaya, Y. S. Kivshar, H. Martin, I. Makasyuk and Z. Chen, Phys. Rev. Lett. **92** (2004) 123903; J. W. Fleischer, G. Bartal, O. Cohen, O. Manela, M. Segev, J. Hudock and D. N. Christodoulides, 2004, *ibid.* **92** (2004) 123904.

[25] T. I. Lakoba and J. Yang, J. Comput. Phys. **226** (2007) 1668; T. I. Lakoba and J. Yang, Stud. Appl. Math. **118** (2007) 153.

[26] N. N. Akhmediev, V. I. Korneev, Yu. V. Kuz'menko, Zh. Eh. Eksp. Teor. Fiz. **88** (1985) 107 [Sov. Phys. JETP **61** (1985) 62]; J. M. Soto-Crespo, D. R. Heatley, E. M. Wright and N. N. Akhmediev, Phys. Rev. A **44** (1991) 636.

[27] G. Iooss and D. D. Joseph, *Elementary Stability and Bifurcation Theory* (Springer-Verlag: New York, 1980).

[28] M. Vakhitov and A. Kolokolov, Radiophys. Quantum. Electron. **16** (1973) 783.

[29] G. D. Peng, B. A. Malomed and P. L. Chu, Phys. Scripta **58** (1998) 149.

[30] B. A. Malomed, Phys. Rev. E **58** (1998) 7928.

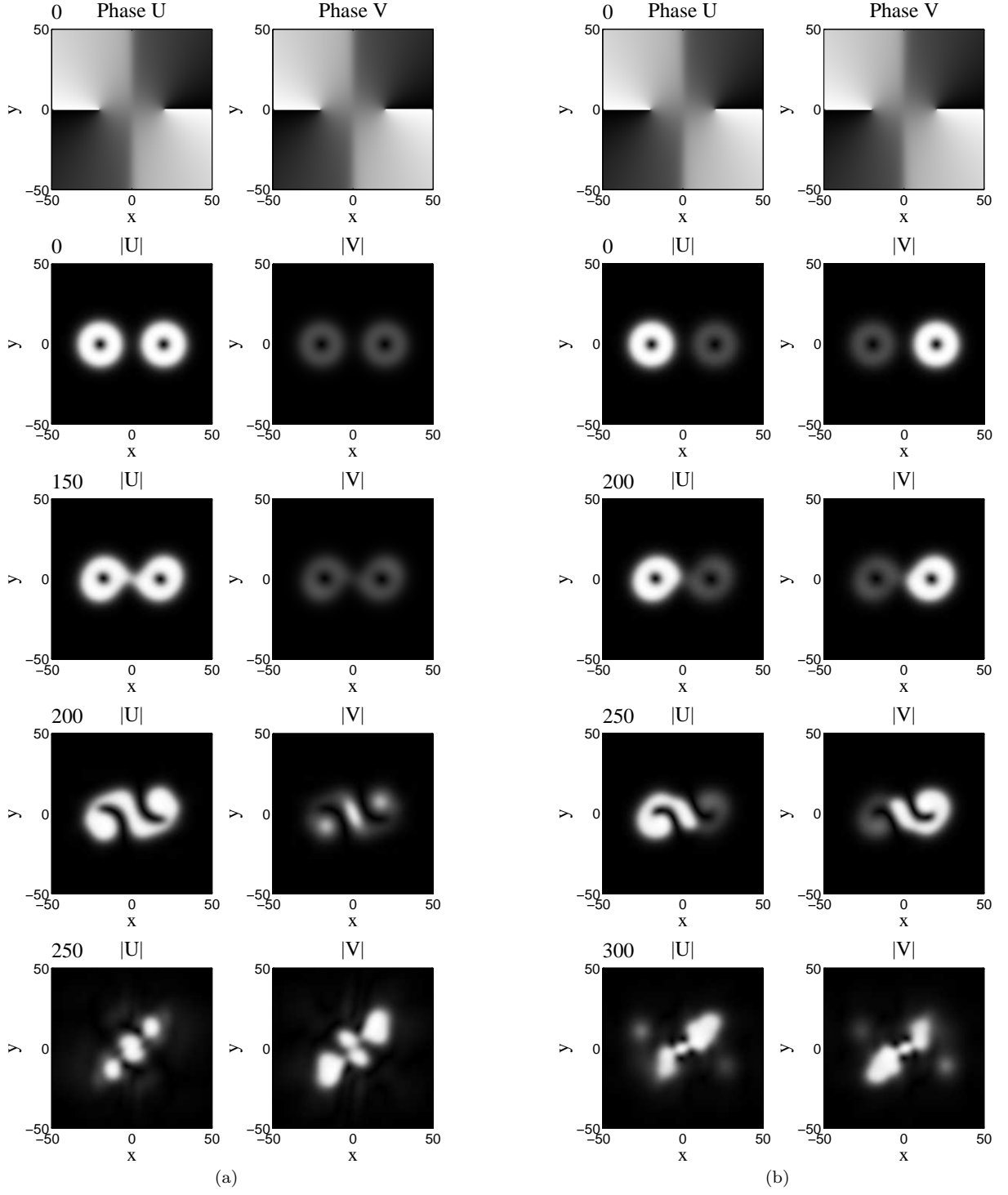[31] D. Mihalache, D. Mazilu, B. A. Malomed, and F. Lederer, Phys. Rev. E **69** (2004) 066614.

FIG. 15. The interaction between asymmetric vortices with $s = 1$, $\Delta\theta = \pi$, $\lambda = 0.05$, $k = 0.18$, and $\Delta x = 40$. Notice the *attraction* between the π-out-of-phase vortex solitons in this case.
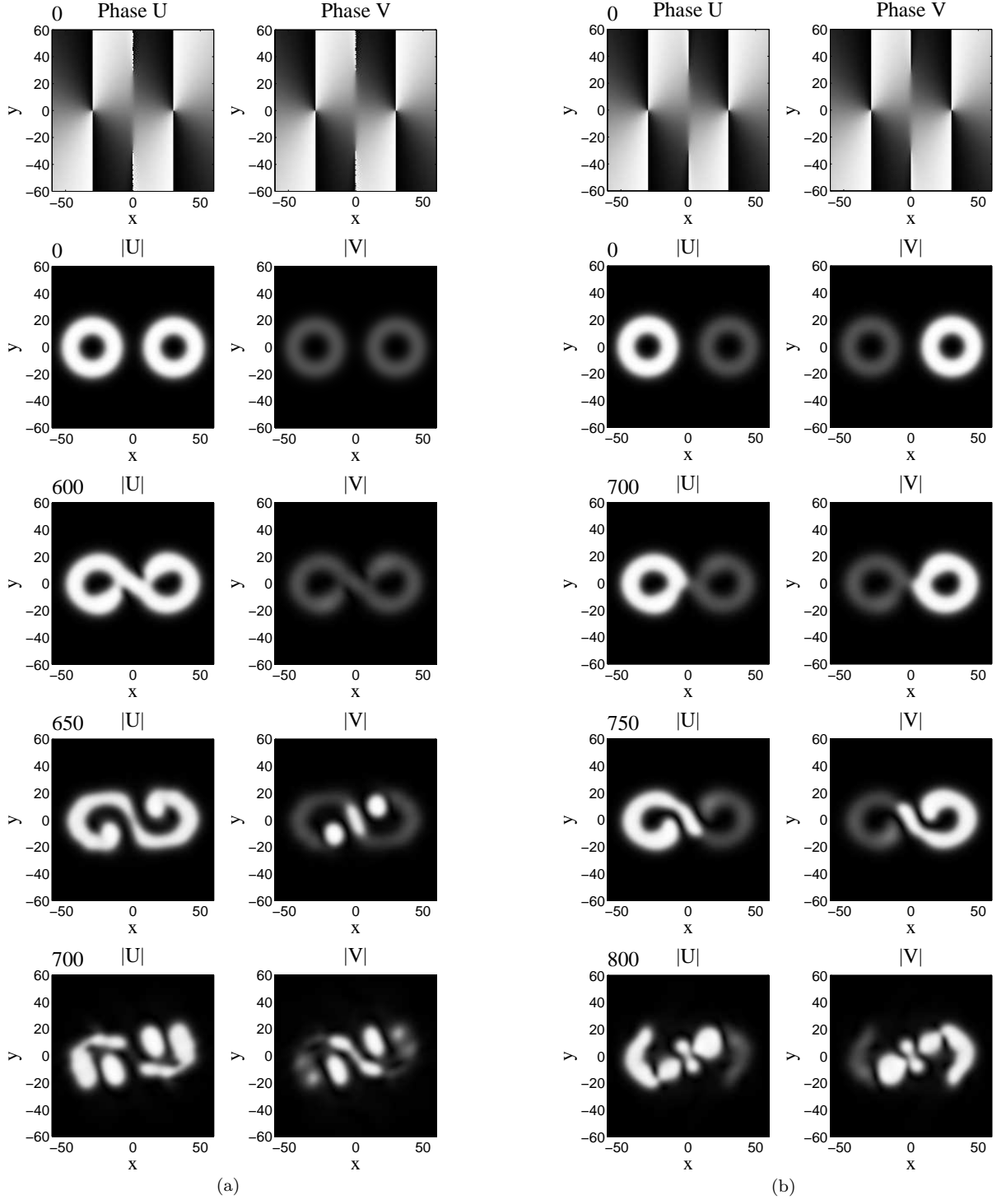
FIG. 16. The interaction between asymmetric in-phase vortices with $s = 2$, $\lambda = 0.05$, $k = 0.184$, and $\Delta x = 60$.
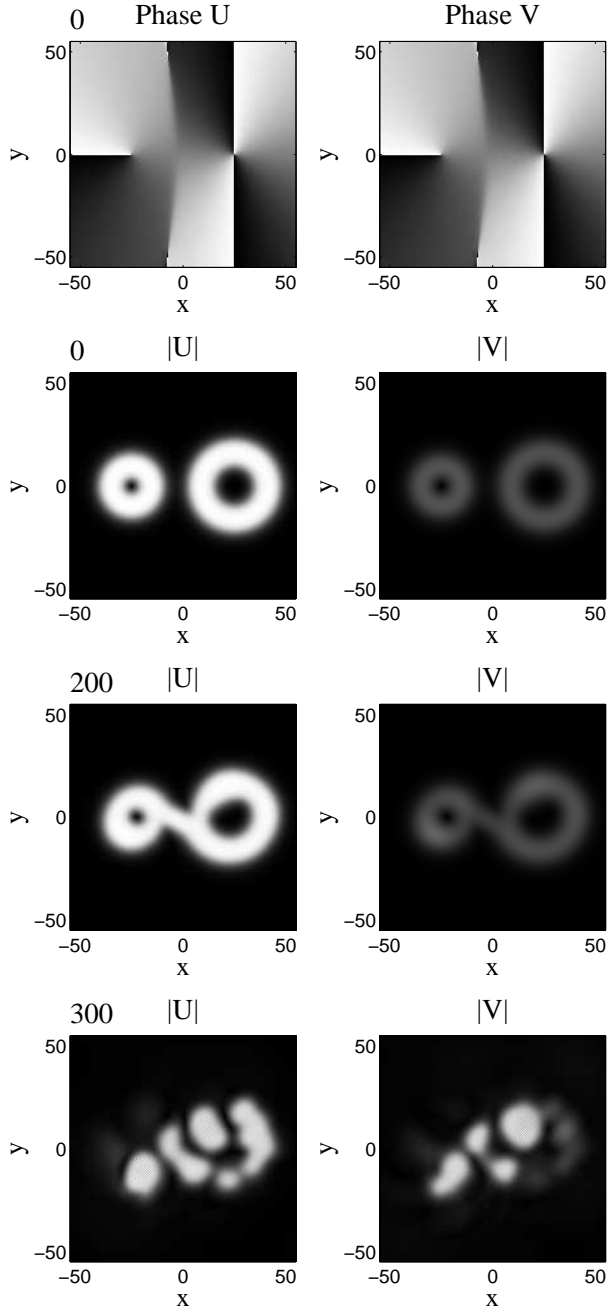
FIG. 17. The interaction between vortices with $s = 1$ and $s = 2$, for $\Delta\theta = 0$, $\Delta x = 50$, and $\lambda = 0.05$, $k = 0.184$.
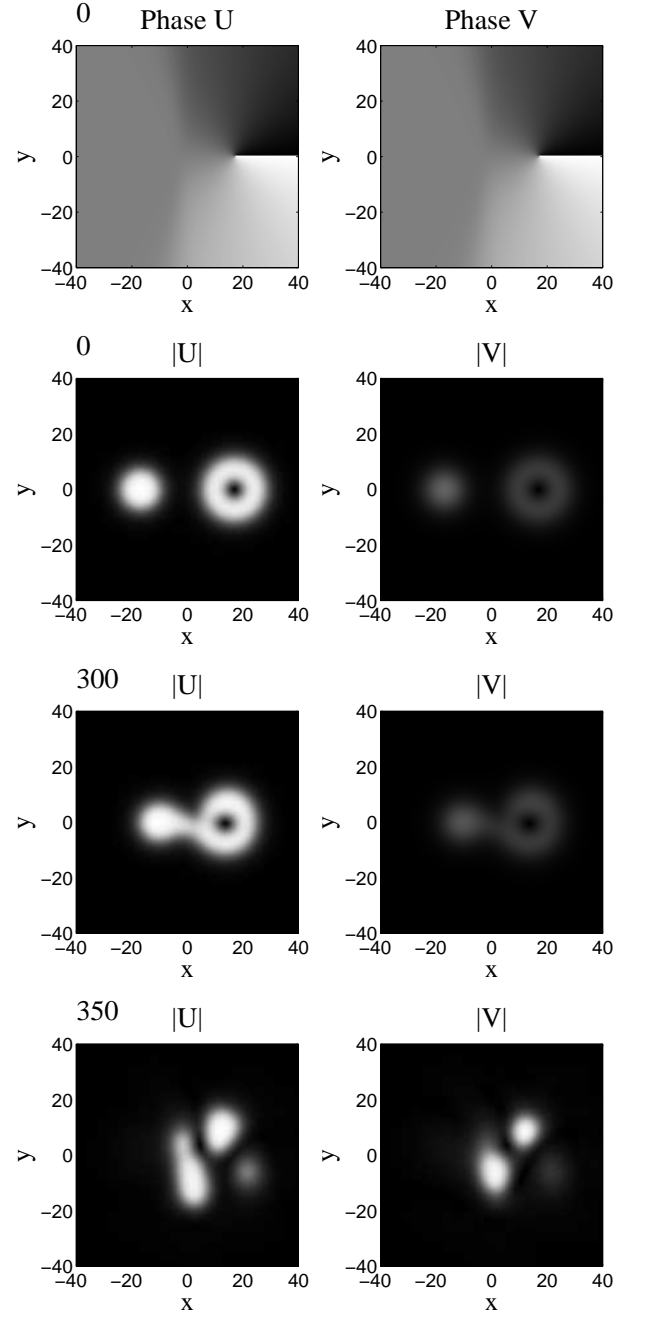
FIG. 18. The interaction between a fundamental soliton $(s = 0)$ and a vortex with $s = 1$, for $\Delta x = 34$, $\Delta\theta = \pi$ and $\lambda = 0.05$, $k = 0.17$.